The noise of coated cantilevers

2012 Nanotechnology 23 025503

(http://iopscience.iop.org/0957-4484/23/2/025503)

IOP PUBLISHING NANOTECHNOLOGY
Nanotechnology **23** (2012) 025503 (9pp) doi:10.1088/0957-4484/23/2/025503

The noise of coated cantilevers

Aleksander Labuda, Jeffrey R Bates and Peter H Grütter

Department of Physics, McGill University, Montreal, H3A 2T8, Canada

Received 9 October 2011, in final form 10 November 2011
Published 14 December 2011
Online at stacks.iop.org/Nano/23/025503

Abstract
In atomic force microscopy, cantilevers with a reflective coating are often used to reduce optical shot noise for deflection detection. However, static AFM experiments can be limited by classical noise and therefore may not benefit from a reduction in shot noise. Furthermore, the cantilever coating has the detrimental side-effect of coupling light power fluctuations into true cantilever bending caused by time-varying thermal stresses. Here, we distinguish three classes of noise: detection, force, and displacement noise. We discuss these noises with respect to cantilever coating in the context of both static and dynamic AFM experiments. Finally, we present a patterned cantilever coating which reduces the impact of these noises.

(Some figures may appear in colour only in the online journal)

1. Introduction

The detection of forces on the atomic scale has been made routine by the advent of microcantilevers now used in most atomic force microscopes (AFM) [1]. Measurements of forces as small as attonewtons have been achieved by the manufacture of specialized cantilevers [2–4], the development of advanced interferometric techniques [5–8] and dedicated optical beam deflection systems [9–11], allowing unprecedented measurements such as single spin detection with nanoscale spatial resolution [12, 13]. Also, functionalized coated cantilevers are used as biochemical detectors based on reaction-induced stress in cantilevers [14–17]. Furthermore, the considerable reduction in detection noise of cantilever deflection [18–22] has enabled atomic-resolution imaging in liquid environments [23–25] which recently culminated in three-dimensional atomic-scale force spectroscopy in liquids [26, 27].

The accuracy in measuring atomic-scale forces relies on proper calibration of the AFM and the determination of the cantilever spring constant, both of which have been the focus of many studies [28–45]. This paper deals with detection noise in cantilever deflection, specifically for the optical beam deflection method [46–56] where a photodetector measures angular changes in a light beam reflected off the cantilever. Furthermore, we clearly distinguish between detection noise, force noise, and displacement noise. This distinction is rarely appreciated and all three noise types are often bundled as a single entity. However, displacement noise and force noise both physically affect the experiment as opposed to the detection noise, which simply limits our ability to measure the bending of the cantilever without actually interfering with the tip–sample physics. Reflective coatings are typically used to reduce the detection noise, but may cause undesirable force and displacement noise. Our analysis aims to understand how a cantilever coating can affect these different noises in the context of static and dynamic [57] AFM modes, with the ultimate goal of minimizing them.

Finally, we present a peculiar cantilever design which reduces all three noise types by its patterned reflective coating shown in figure 1.

2. Noise classification

In this section, we discuss the phenomenological classification of AFM noise into three categories: detection noise, force noise, and displacement noise. This classification is based on how a noise source affects the AFM measurement, regardless of the physical origin of that noise.

A single noise source can manifest itself in all three noise classes for a static AFM experiment. Consider the infamous 60 Hz line noise which affects experiments in the Americas. A 60 Hz modulation of the detection light beam power can affect the measurement of the cantilever deflection without disturbing the tip–sample physics; this ‘false deflection’ is a detection noise. However, if the cantilever is coated, the same 60 Hz modulation in optical power can cause stress-induced cantilever bending due to a difference in thermal expansion coefficients. The resulting 60 Hz force modulation of the cantilever is a force noise. On the other hand, 60 Hz noise

Figure 1. A gold-coated 500 μm-long arrow TL2 cantilever was machined by focused ion beam (FIB) to remove sections of the gold coating; the exposed silicon appears darker in this image. The upper cantilever remained unmodified and was used as a control. The Fresnel pattern milled into the cantilever can be used to reduce the detection noise. Removing gold from the rest of the cantilever body has the added benefit of reducing the time-varying fluctuations of the cantilever induced by thermal stress.

in the piezoscanner cable can cause a displacement of the sample. This would result in a true tip–sample distance modulation—a displacement noise.

Note that force noise is perceivable as a cantilever deflection before contact with the sample, while displacement noise only becomes perceivable once tip–sample contact is made. Nevertheless, these noises remain present throughout the entire experiment, and can affect the tip–sample physics even if they are not detected as a cantilever deflection.

In the following three sections, we investigate the three noise classes in greater detail, but restrict the discussion to noise sources which relate to the cantilever reflective coating.

2.1. Detection noise

The angular detection noise density n_θ, in rad $\text{Hz}^{-1/2}$, describes the lower detection limit for an optical beam deflection system across any arbitrary bandwidth [19]. The angular bending of the cantilever can in principle be calibrated into a tip displacement and a force; however, we avoid complications that arise around and above the cantilever resonance frequency, discussed elsewhere [58–61], by simply dealing with the unequivocal angular detection noise density n_θ to describe detection noise in this paper.

For small cantilever deflections, n_θ can be estimated empirically by shining the light beam off the rigid cantilever chip and measuring the noise density $n_{\Delta P}$ (W $\text{Hz}^{-1/2}$) of the deflection signal ΔP and then calibrating by

$$n_\theta = \frac{n_{\Delta P}}{S_\theta}, \tag{1}$$

where the angular deflection sensitivity S_θ (W rad^{-1}) is a property of the reflected light beam, as will be explained below. Note that this calibration procedure avoids measurement of the thermal response of the cantilever, which is not a detection noise as it relates to true cantilever bending and therefore is a force noise.

To first order S_θ scales proportionally to the optical power P at the photodetector. This suggests that cantilevers with a reflective coating should provide lower detection noise over uncoated cantilevers. However, this general rule-of-thumb does not always apply, for reasons which can be understood by investigating S_θ and $n_{\Delta P}$ more closely.

The sensitivity S_θ is proportional to the irradiance at the center of the photodetector I_0 by

$$S_\theta = 4I_0, \tag{2}$$

where a factor of 2 emerges because a cantilever deflection doubles the reflection angle, and the remaining factor of 2 exists because ΔP measures the difference in power between the two sections of the split photodetector. This irradiance I_0 is not only a function of P, but is also inversely proportional to the divergence of the light beam reaching the photodetector [62] (in the case of a Gaussian beam). This divergence can be strongly affected by the stress-induced cantilever curvature caused by the reflective coating, for example, which can increase or decrease n_θ disregarding changes in P [19].

Secondly, the noise density is actually composed of three different types of noise and each scales differently with optical power P [63, 64]:

(1) classical noise is caused by angular fluctuation in the light beam, $n_{\Delta P,\text{clas}} \propto P$;
(2) optical shot noise is due to the counting statistics of the photons, $n_{\Delta P,\text{shot}} \propto \sqrt{P}$;
(3) electronic noise is caused by imperfect detection electronics, $n_{\Delta P,\text{elec}} \propto 1$. It is listed here for completeness, but its contribution can be made negligible by designing appropriate detection electronics [18, 58] and it will be ignored henceforth.

Finally, the revised version of equation (1) becomes

$$n_\theta = \frac{\sqrt{n^2_{\Delta P,\text{clas}} + n^2_{\Delta P\text{shot}}}}{4I_0}. \tag{3}$$

In a typical AFM setup, increasing P by a reflective coating has no effect on the classical noise component of n_θ because both the numerator and denominator scale linearly with P. Therefore, static AFM experiments that are limited by classical noise, such as $1/f$ noise [65–67], do not benefit from a reflective coating; in fact, section 2.2 explains how a coating can be detrimental to an AFM experiment.

Section 3 describes how the Fresnel cantilever in figure 1 can counterintuitively increase the irradiance I_0 by discarding optical power P—both of which reduce n_θ.

2.2. Force noise

Although the stochastic thermal driving force of a cantilever, related to viscous damping [68–73], is a force noise, we disregard it from this discussion as it only weakly depends

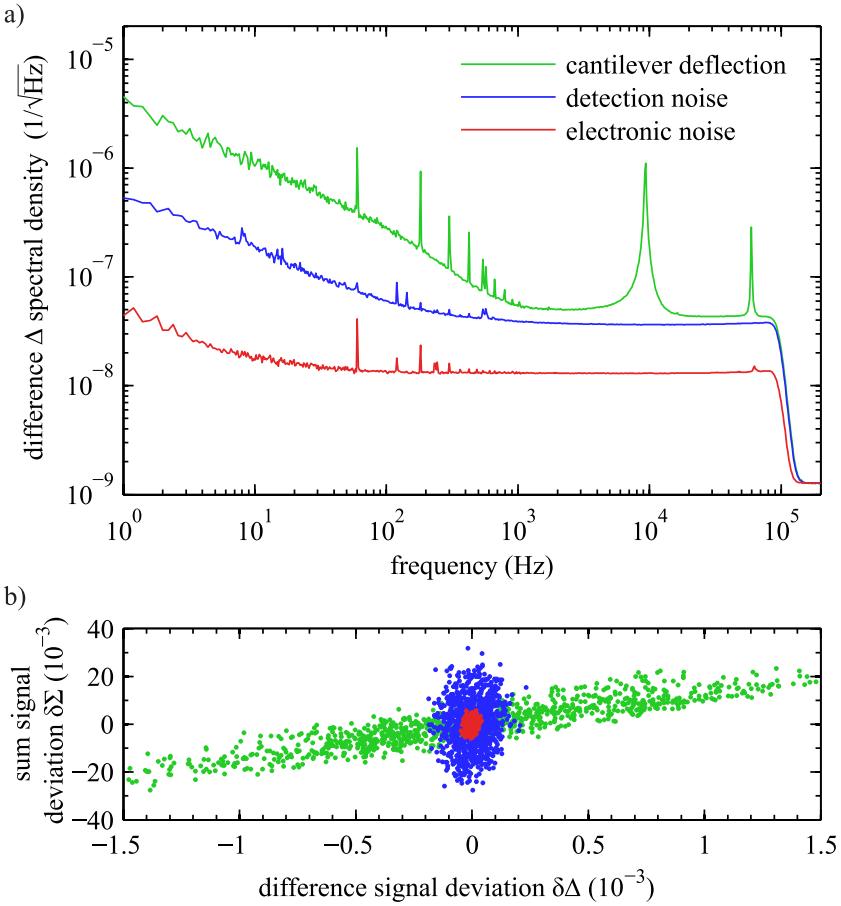

Figure 2. (a) The thermal spectrum of a tip-side coated silicon cantilever was acquired by measuring the (normalized) difference signal Δ from the photodetector. The detection noise, measured by reflecting the light off the solid cantilever chip, and the electronic noise are also shown. The cantilever deflection has a well resolvable $1/f$ spectrum. (b) A correlation plot between the normalized sum signal (total light power) deviations and the normalized difference signal deviations for the three measurements shown in (a) demonstrates a strong correlation between the $1/f$ cantilever deflection and the $1/f$ fluctuations of the light beam power. The signals were downsampled to 100 Hz.

on the cantilever coating in viscous media. In vacuum environments, where forces are usually measured using frequency modulation AFM [74], the cantilever coating can cause a significant reduction of the Q-factor [75–78] with an associated increase in force noise [79–84]. These effects have been extensively studied and will not be investigated further.

In static AFM, two mechanisms of force noise related to the coating can be prominent and problematic. As described earlier, fluctuations in the total optical power P incident on the cantilever may cause a time-varying stress on the cantilever due the difference in thermal expansion coefficients of the cantilever bulk and the reflective coating. Secondly, the viscoelastic damping due to the cantilever coating can be a source of $1/f$ force noise [85–87]. Also known as structural damping, viscoelastic damping carries a different spectral distribution from the well-known viscous damping because it appears as a complex component of stiffness when considering the equation of motion of a cantilever.

In our system, the force noise caused by thermal stress dominates over the viscoelastic damping noise. Figure 2 demonstrates that the cantilever deflection signal is strongly correlated to the light power signal, implying that the $1/f$ fluctuations in light power cause cantilever deflections via the thermal-stress mechanism. Also note that the cantilever bending is modulated by 60 Hz and harmonics, even though our detection system has no 60 Hz noise.

This force noise can be quantified by some time-varying stress per unit length $\sigma(t)$ acting along the coated portions of the cantilever. For a fully coated cantilever, with a uniform cross-section, a force fluctuation δF caused by a stress fluctuation $\delta\sigma$ can be determined by integrating along the cantilever:

$$\delta F \propto \int_0^L \delta\sigma \, \mathrm{d}x = L\delta\sigma, \tag{4}$$

where x is the distance along the cantilever of full length L.

This integral suggests that the force noise scales proportionally to the area of the cantilever which is covered in the reflective coating. In this regard, the patterned cantilever in figure 1 is expected to have 4.0× less force noise than the fully coated cantilever.

Note that equation (4) is valid under the assumption that the stress fluctuations $\delta\sigma$ at all positions $\mathrm{d}x$ are identical, which is a good approximation for stress induced by temperature changes of the cantilever at low frequencies, where the thermal diffusion length [88, 89] is comparable to the cantilever length. Note that the $1/f$ thermal fluctuations observed in figure 2 begin to roll off above 200 Hz as this

assumption begins to break down. Also, equation (4) is only valid in the situation where a feedback system maintains a constant angular deflection, which is the case for AFM imaging using an optical beam deflection system.

2.3. Displacement noise

In contrast to static AFM, the coating-induced cantilever deflection fluctuations cause only displacement noise in the case of dynamic AFM. This change in noise classification of the same noise source stems solely from a bandwidth argument. Because forces measured by dynamic AFM are encoded as changes in frequency, amplitude, or phase at high driving frequencies, they are not directly affected by the low-frequency cantilever fluctuations related to the reflective coating. Instead, this bending of the cantilever causes the 'zero-force deflection point' z_0 to change with time according to a $1/f$ and 60 Hz spectrum. This problem effectively results in a time-varying tip–sample distance, which justifies its classification as a displacement noise. In topography imaging, these fluctuations in δz_0 are compensated by the imaging feedback loop and erroneously recorded as changes in topography. They scale as

$$\delta z_0 \propto \int_0^L (L-x)\delta\sigma \, \mathrm{d}x = \frac{L^2 \Delta\sigma}{2}. \tag{5}$$

The $(L-x)$ factor in this integration represents the lever arm which relates an angular bending of the cantilever to a normal deflection at the tip apex. For example, angular bending at the cantilever apex causes nearly no displacement of the cantilever tip, whereas angular bending at the cantilever base has a lever arm of length L, therefore causing large tip displacement.

This fact suggests that removing reflective coating near the base of the cantilever reduces the displacement noise to a far greater extent than removing coating near the apex. This also implies that the benefits of a patterned coating as in figure 1 can be especially notable for displacement noise in dynamic AFM. In fact, the patterned cantilever in figure 1 is expected to have 7.7× less displacement noise than the fully coated cantilever.

3. Fresnel cantilever design

In this section, we use Fraunhofer diffraction theory [90] to derive the irradiance at the photodetector center I_0 and the total optical power P as a function of the amplitude profile of the light beam reflected off the cantilever, and then use the Fresnel lens principle [91] to maximize I_0 by reducing P. As described in section 2.1, these two values determine the detection noise of the AFM. Whereas the basic principle behind the Fresnel cantilever will be presented in this section, the reader is referred to the appendix for more specific technical details. The performance of the Fresnel cantilever with regard to detection, force and displacement noise will be assessed in section 3.3.

3.1. Fraunhofer diffraction in AFM

Fraunhofer diffraction theory suffices for explaining the behavior of light as it travels from the cantilever to the photodetector, because the latter is in the far-field in nearly all AFM designs. In the context of AFM, Fraunhofer diffraction can be summarized by the following statement: the angular distribution of the far-field irradiance $I_{\mathrm{FF}}(\theta')$, where θ' is the angular coordinate of the diffracting light beam, is the square of the Fourier transform of the complex-valued amplitude profile $A_{\mathrm{R}}(x)$ reflected off the cantilever, where x is the distance along the cantilever. Mathematically [92],

$$I_{\mathrm{FF}}(\theta') = \frac{1}{\lambda}\left|\int_0^L A_{\mathrm{R}}(x)\mathrm{e}^{-\mathrm{i}k\theta' x}\,\mathrm{d}x\right|^2, \tag{6}$$

where $k = 2\pi/\lambda$ is the wave vector for a wavelength λ. Note that the irradiance in the far-field $I_{\mathrm{FF}}(\theta')$ has units of W rad^{-1} that are appropriate as the optical beam deflection system detects an *angular* change in the cantilever. The Fourier conjugate relationship in equation (6) reminds us of the fact that a larger spot size on the cantilever causes a smaller spot size at the photodetector thereby leading to increased sensitivity [93]. For small cantilever deflections, the sensitivity is simply proportional to $I_0 \equiv I_{\mathrm{FF}}(\theta' = 0)$.[1]

In small-deflection AFM, we are only interested in I_0, such that the Fourier transform in equation (6) can be simplified by setting $\theta' = 0$:

$$I_0 = \frac{1}{\lambda}\left|\int_0^L A_{\mathrm{R}}(x)\,\mathrm{d}x\right|^2. \tag{7}$$

Interestingly, to first order, the deflection sensitivity in AFM is simply proportional to the squared integral of the amplitude profile reflected off the cantilever. Spreading the intensity profile of the light beam across a larger area of the cantilever can increase the value of this integral because of the nonlinear relationship between intensity and amplitude.

Finally, determination of the total optical power P is trivial:

$$P = \int_0^L |A_{\mathrm{R}}(x)|^2\,\mathrm{d}x. \tag{8}$$

Now I_0 and P can be optimized for the reduction of detection noise n_θ.

3.2. Fresnel cantilever: basic principle

This section explains how the Fresnel pattern in figure 1 can increase the irradiance at the center of the photodetector I_0 while minimizing the total optical power P.

Figure 3(a) demonstrates a common AFM scenario, where a Gaussian light beam is focused onto a gold-coated silicon cantilever. At the focus, the phase profile of a Gaussian

[1] This only strictly applies if $A_{\mathrm{R}}(x)$ is symmetric, which we assume herein. In the more general case, I_0 is defined as the irradiance at the photodetector center when half of the optical power resides on either side of the photodetector. This may occur at $\theta' \neq 0$ if $A_{\mathrm{R}}(x)$ is complex-valued and asymmetric.

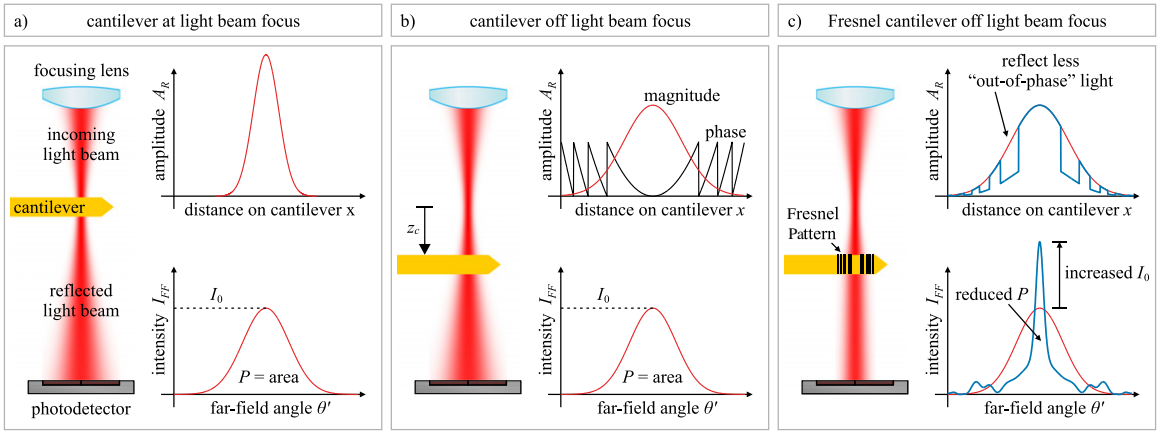

Figure 3. (a) This diagram depicts the detection scheme for a cantilever in a regular setup, where the light beam is focused onto the cantilever. The amplitude profile reflected off the cantilever A_R is shown in the top graph; the intensity distribution I_{FF} on the photodetector in the far-field is shown below. The peak intensity and the total power P determine the detection noise. (b) Moving the cantilever away from the focus by a distance z_c increases the reflected beam diameter. This does not affect the detection noise because the (apparent) benefit of a larger beam diameter is negated by the phase profile, which makes some of the reflected light amplitude destructively interfere at the photodetector in the far-field. (c) Patterning the cantilever by removing some gold reduces the magnitude of the 'out-of-phase' light which destructively interferes at the photodetector. This reduces detection noise because both I_0 is increased and P is reduced.

beam is uniform, and therefore the reflected amplitude profile is simply

$$A_R(x) = \sqrt{I_G(x)}, \tag{9}$$

where $I_G(x)$ is the irradiance profile of the incident Gaussian beam. By equation (6), the Fourier transform of this amplitude profile results in a Gaussian profile at the photodetector—also shown in figure 3(a).

Positioning the cantilever at some axial distance z_c away from the light beam focus causes the reflected light beam diameter to increase, as shown in figure 3(b). As long as no light spills over the cantilever edges, changing z_c has no consequence on the intensity distribution in the far-field or on the detection noise—to first order. Although the reflected beam diameter is larger in figure 3(b), the irradiance in the far-field $I_{FF}(\theta')$ remains identical to that in the previous case. This invariance to z_c is due to the variable phase profile of the complex-valued amplitude $A_R(x)$ which encodes the information about the beam divergence at any position z_c. In fact, the reflected amplitude profile for an arbitrary z_c is

$$A_R(x|z_c) = \sqrt{I_G(x|z_c)}e^{i\phi_G(x|z_c)}, \tag{10}$$

where, by the paraxial approximation [94], the phase profile can be modeled as parabolic:

$$\phi_G(x|z_c) = \frac{kx^2}{2R(z_c)'}, \tag{11}$$

where $R(z_c)$ is the wavefront radius of curvature. The focus ($z_c = 0$) is a special case where a planar wavefront ($R = \infty$) causes a flat phase profile, as seen in figure 3(a); anywhere else, the radius of curvature is given by

$$R(z_c) = z_c\left[1 + \left(\frac{z_R}{z_c}\right)^2\right]. \tag{12}$$

where the smallest radius is obtained at the Rayleigh range z_R, defined as the distance from the focus where the light beam area is doubled.

We now turn our attention to the single 'Fraunhofer integration' of I_0 in equation (7), which we would like to maximize to reduce detection noise. The irradiance I_0 is independent of z_c because different locations of $A_R(x|z_c)$ constructively or destructively interfere during its integration, thereby maintaining a fixed I_0 even though the reflected beam diameter increases. Therefore, in the case of $z_c \neq 0$, we can conclude that certain sections of the amplitude profile in figure 3(b) are actually detrimental to the detection noise, as they reduce I_0 by destructive interference. Discarding these sections of 'out-of-phase' amplitude should increase I_0, with an added benefit of decreasing the total optical power P.

This task is fulfilled by the Fresnel cantilever, as shown in figure 3(c). Removing the gold coating in chosen sections significantly reduces the reflectance, thereby partially discarding 'out-of-phase' amplitude. As seen in figure 3(c), the irradiance in the far-field is far from Gaussian, but the goal of increasing I_0 and reducing P is achieved by the Fresnel cantilever. Mathematically, the reflected amplitude in this case is

$$A_R(x|z_c) = r(x)\sqrt{I_G(x|z_c)}e^{i\phi_G(x|z_c)+i\phi_R(x)}, \tag{13}$$

where the reflectance profile $r(x)$ and the phase profile $\phi_R(x)$ account for differences between the reflection from gold and silicon sections of the Fresnel pattern. This phase difference $\phi_R(x)$ is caused by both phase changes upon reflection from gold and silicon, as well as the path difference due to the finite thickness of the gold coating.

3.3. Fresnel cantilever: proof-of-principle

Ideally, a Fresnel cantilever would be fabricated at the wafer level, with appropriate mask patterning. This process is only

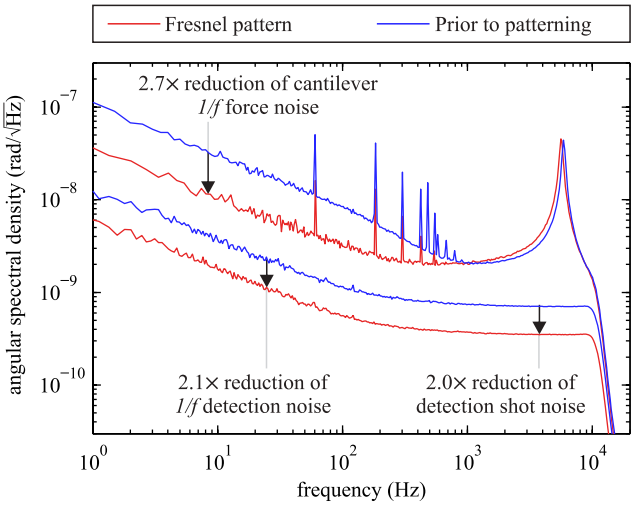

Figure 4. The thermal spectrum of the cantilever was measured before and after Fresnel patterning (two upper curves). The detection noise was also measured in both situations (two lower curves). The arrows point out the 2.7× reduction in cantilever $1/f$ force noise, the 2.1× reduction in $1/f$ detection noise, and the 2.0× reduction in detection shot noise attributable to the Fresnel pattern. Note that our detection system has no 60 Hz noise, however our cantilever vibrates with 60 Hz and harmonics.

cost effective for large volumes. For this reason, we have used a focused ion beam (FIB) to construct our proof-of-principle Fresnel cantilever, presented in figure 1.

For a regular cantilever, the AFM user typically maximizes the reflected light power before starting an experiment. For a Fresnel cantilever, this approach is ineffective as the idea is to *reduce* the reflected light power in order to maximize the sensitivity. Experimentally, the location of the light beam on the Fresnel cantilever is optimized as follows: first, the light beam is defocused by the height z_c and roughly centered on the Fresnel pattern; then, the light beam lateral position is manually adjusted to maximize the driven response of the cantilever using a lock-in measurement.

Removing 75% of the gold coating on the cantilever in figure 1 reduced the $1/f$ force noise by 2.7×, as can be seen in figure 4. This is less than the expected reduction of 4.0×. We attribute a large part of the discrepancy to the FIB implantation of gallium ions that caused a stress-induced cantilever bending [95] which can be temperature dependent.

The reduction in displacement noise could not be observed directly because the optical beam deflection measurements are only sensitive to angular changes of the cantilever. According to the theory presented in sections 2.2 and 2.3, the observed 2.7× reduction in force noise should correspond to roughly a 5.2× reduction in displacement noise at low frequencies.

The Fresnel pattern was expected to reduce the detection noise by 3.8× and 3.4× for classical noise and shot noise respectively (see appendix for details). The resulting reductions in noise were 2.1× and 2.0×. Some of this discrepancy is due to the curvature of the cantilever, which was not considered when designing the Fresnel cantilever. Secondly, the implanted gallium ions from FIB milling can increase the silicon reflectivity [96], and therefore reduce the effectiveness of the Fresnel pattern. Measuring the reflectivity of the FIB-milled areas versus the gold-coated areas confirms this suspicion: the reflectivity of the FIB-milled area drops to 65% of the coated area reflectivity (rather than the 34% expected for bare silicon).

Despite the differences between theory and experiment, which are expected to be predominantly caused by the FIB milling process, these proof-of-principle cantilevers demonstrate that patterned coatings on cantilevers can be used to reduce detection noise by taking advantage of the reflectivity contrast and by tuning the coating thickness (the importance of the coating thickness is elaborated upon in the appendix). Also, removing the coating in unnecessary areas of the cantilever can reduce force noise and corresponding displacement noise.

4. Summary

In static AFM experiments, a reflective cantilever coating couples fluctuations of the light beam power into a true cantilever deflection caused by time-varying thermal stresses. In other words, the coating increases the force noise. Stripping the coating from locations of the cantilever which do not reflect light reduces the impact of the problem.

Reflective coatings are typically used to reduce detection noise; however, the coating does not reduce classical detection noise (such as $1/f$ noise) which exceeds shot noise below a certain cut-off frequency. On the other hand, all sources of noise scale with the divergence of the reflected light beam, because a beam more focused onto the photodetector causes a larger signal for a given change in cantilever angle. This can be achieved by patterning the cantilever, such that the coating acts as a Fresnel lens to focus the reflected light beam.

It is interesting to note that the 60 Hz noise (and harmonics) observed in the thermal spectrum of the cantilever (in figures 2 and 4) is actually force noise, not detection noise. This noise arises due to modulation of the light beam which causes stress-induced bending of the cantilever. On the other hand, the same modulation of the light power does not affect the detection noise because of the differential nature of the deflection measurement. Although it is tempting to filter out or ignore 60 Hz noise by assuming it is a detection noise, this does not resolve the problem as the 60 Hz modulation is a real and measurable modulation of tip–sample forces that can affect the tip–sample physics.

In dynamic AFM experiments, low-frequency detection noise is omitted by measuring the oscillation of the cantilever at high frequency, near its resonance. In this case, detection noise is dominated by optical shot noise, which can also be reduced by a Fresnel pattern.

Importantly, the same stress-induced cantilever bending that causes force noise in static AFM actually causes displacement noise in dynamic AFM experiments. The 60 Hz force noise discussed above appears as a true tip–sample distance modulation in this case. This displacement noise can also be reduced by removal of unnecessary reflective coating.

Acknowledgments

We acknowledge valuable discussions with Mark Sutton, Kei Kobayashi, Srikar Vengallatore and Jessica Topple, as well as Jason Cleveland, Deron Walters, and Mario Viani from Asylum Research. We thank George McMurtry from NanoAndMore for providing cantilevers. Funding from NSERC and FQRNT is gratefully acknowledged. FIB machining was performed at École Polytechnique de Montréal.

Appendix

A.1. Construction of a Fresnel cantilever

The optimization of the Fresnel pattern requires a proper characterization of the incoming light beam. Figure A.1(a) shows the irradiance profile of the incoming light beam in our home-built AFM [58]. It was acquired by shining the collimated light beam directly onto the sensor of a digital camera (D700, Nikon, Japan). A Gaussian fit reveals that the one-dimensional intensity profile deviates from Gaussian by no more than 3% within the beam diameter. Knowing the collimated beam diameter (2.2 mm), the effective focal length (19.0 mm) of the focusing lens and the wavelength (680 nm) provide the necessary information for modeling the incoming light beam. The target height z_c of the cantilever from the light beam focus was selected such that the beam diameter matched the cantilever width of 100 μm upon reflection: $z_c = 0.86$ mm. This semi-arbitrary choice maximizes the beam diameter incident on the cantilever while reducing unwanted loss of light.

Figure A.1(b) shows the amplitude profile of the incident light beam. The thick lines denote the 'out-of-phase' amplitude portions which were deemed detrimental to detection shot noise. A brute force method was used to determine the minimum and maximum angles of this 'out-of-phase' range: the shot noise for every combination of minimum and maximum phase angles was numerically computed to determine the optimal angle range resulting in the highest irradiance at the photodetector center I_0.

Unlike a regular Fresnel lens [97], the Fresnel cantilever used here is binary: the locations of the reflection profile can be either gold or silicon. As shown in figure A.1(c), the silicon is used to partially discard the 'out-of-phase' light because its reflectance is much lower than that of gold ($r_{Si} = 0.58$ versus r_{Au}) [98, 99].

There is an added benefit to the fact that the phase shift upon reflection differs between the two materials: the light deemed 'out-of-phase' which still reflects off the silicon due its partial reflectance undergoes a phase shift which makes it interfere less destructively during the integration of I_0 in equation (7). The phase shifts upon reflection for the two materials are $\phi_{Si} = 179°$ and $\phi_{Au} = 149°$ [100].

The relative phase shift upon reflection from both materials also changes due to a geometric effect. The height difference $\Delta z = 50$ nm between the layer of gold and the

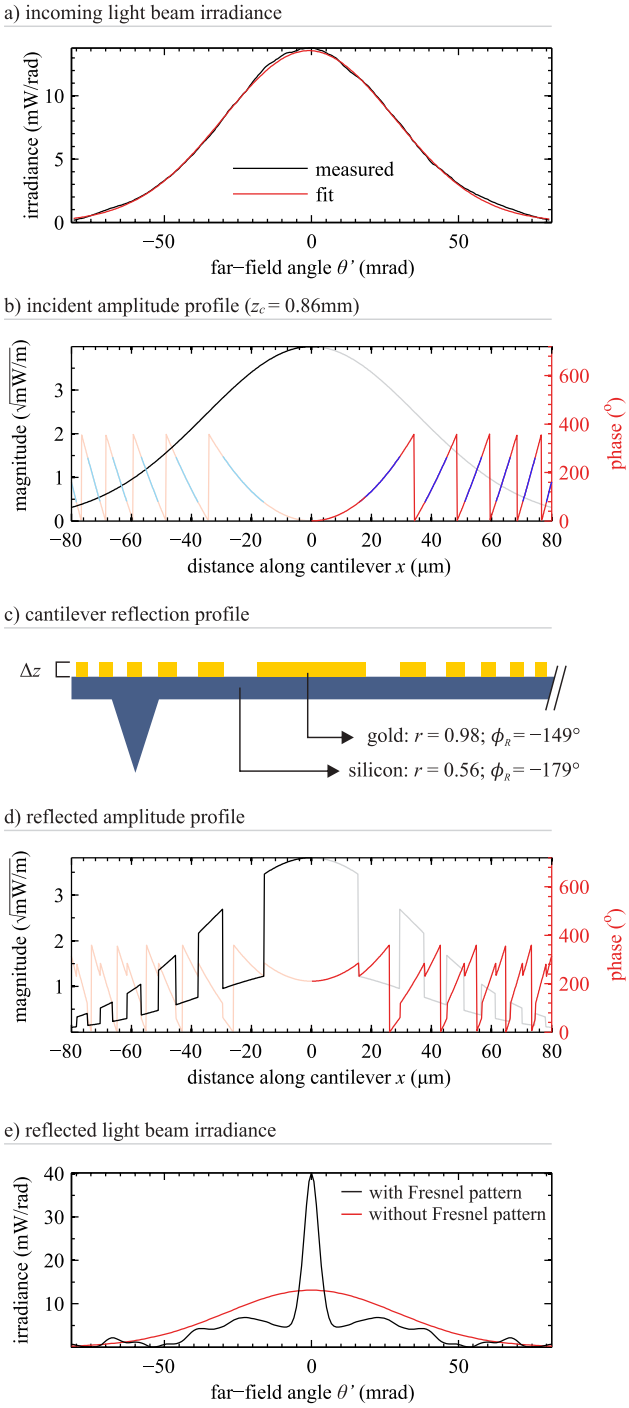

Figure A.1. (a) The incoming far-field irradiance was measured on our AFM, and fitted to a Gaussian with very good agreement. (b) The amplitude profile incident on the cantilever (0.86 mm away from the light beam focus) is shown by its magnitude and phase; both profiles were faded for visual clarity on the right and left sides, respectively. The phase profile portions in blue are deemed detrimental to the detection noise, and should be discarded. (c) The gold coating on the cantilever is patterned to discard the portions of light deemed detrimental. (d) The amplitude profile after reflection from the patterned cantilever. (e) The far-field irradiance for a gold-coated cantilever with and without a Fresnel pattern. The pattern increases the irradiance in the center I_0, while reducing the total optical power P.

silicon causes an optical path difference and an additional phase shift given by the ratio $2\Delta z/\lambda$.

The full reflection profile of the Fresnel cantilever is represented in figure A.1(c). The amplitude profile $A_R(x, z_c)$ reflected off the cantilever is shown in figure A.1(d). Finally, the irradiance profile in the far-field for this Fresnel cantilever was calculated by inserting $A_R(x)$ from equation (13) into equation (6), and is shown in figure A.1(e). The resulting irradiance I_0 is 3.8× larger than for a regular gold-coated cantilever, thereby reducing the classical noise δz_{clas} by the same factor. The shot noise δz_{shot} was reduced because of the power lost (∼22%) by adsorption and transmission through the silicon.

A second simulation was performed (not shown) that demonstrates a reduction of 6.4× for classical noise and 5.8× for shot noise if the gold to silicon height is optimized to $\Delta z \sim 150$ nm. This value is close to $\lambda/4$, which causes a path length difference of roughly $\lambda/2$, thereby bringing the 'out-of-phase' light back into phase with the rest of the light beam. This suggests that the coating height is an important tuning parameter for optimization of the Fresnel pattern.

References

[1] Binnig G, Quate C F and Gerber Ch 1987 *Phys. Rev. Lett.* **56** 930–3
[2] Stowe T D, Yasumura K, Kenny T W, Botkin D, Wago K and Rugar D 1997 *Ultramicroscopy* **71** 288–90
[3] Stowe T D, Yasumura K Y, Kenny T W, Botkin D, Wago K and Rugar D 1997 *Appl. Phys. Lett.* **71** 288
[4] Nellen P M, Callegari V and Sennhauser U 2006 *Chimia* **60** 735–41
[5] Rugar D, Mamin H J and Guethner P 1989 *Appl. Phys. Lett.* **55** 2588
[6] Hoogenboom B W *et al* 2005 *Appl. Phys. Lett.* **86** 074101
[7] Smith D T, Pratt J R and Howard L P 2009 *Rev. Sci. Instrum.* **80** 035105
[8] Rasool H I, Wilkinson P R, Stieg A Z and Gimzewski J K 2010 *Rev. Sci. Instrum.* **81** 023703
[9] Labuda A, Brastaviceanu T, Pavlov I, Paul W and Rassier D E 2011 *Rev. Sci. Instrum.* **82** 013701
[10] Rast S, Gysin U, Ruff P, Gerber Ch, Meyer E and Lee D W 2006 *Nanotechnology* **17** S189–94
[11] Gysin U, Rast S, Kisiel M, Werle C and Meyer E 2011 *Rev. Sci. Instrum.* **82** 023705
[12] Degen C L, Poggio M, Mamin H J, Rettner C T and Rugar D 2009 *Proc. Natl Acad. Sci. USA* **106** 1313–7
[13] Rugar D, Budakian R, Mamin H J and Chui B W 2004 *Nature* **430** 329–32
[14] Gimzewski J K, Gerber Ch, Meyer E and Schlittler R R 1994 *Chem. Phys. Lett.* **217** 589–94
[15] Berger R *et al* 1997 *Science* **276** 2021–4
[16] Godin M, Tabard-Cossa V, Miyahara Y, Monga T, Williams P J, Beaulieu L Y, Bruce Lennox R and Grutter P 2010 *Nanotechnology* **21** 75501
[17] Fritz J *et al* 2000 *Science* **288** 316–8
[18] Fukuma T, Kimura M, Kobayashi K, Matsushige K and Yamada H 2005 *Rev. Sci. Instrum.* **76** 053704
[19] Labuda A and Grütter P H 2011 *Rev. Sci. Instrum.* **82** 013704
[20] Fukuma T, Kimura M, Kobayashi K, Matsushige K and Yamada H 2005 *Rev. Sci. Instrum.* **76** 053704
[21] Fukuma T and Jarvis S P 2006 *Rev. Sci. Instrum.* **77** 043701
[22] Fukuma T 2009 *Rev. Sci. Instrum.* **80** 023707
[23] Fukuma T, Kobayashi K, Matsushige K and Yamada H 2005 *Appl. Phys. Lett.* **87** 034101
[24] Hoogenboom B W, Hug H J, Pellmont Y, Martin S, Frederix P L T M, Fotiadis D and Engel A 2006 *Appl. Phys. Lett.* **88** 193109
[25] Asylum Research 2011 www.asylumresearch.com/News/News.shtml#PointDefects
[26] Labuda A, Kobayashi K, Kiracofe D, Suzuki K, Grütter P H and Yamada H 2011 *AIP Adv.* **1** 022136
[27] Fukuma T, Ueda Y, Yoshioka S and Asakawa H 2010 *Phys. Rev. Lett.* **104** 2–5
[28] Proksch R, Schäffer T E, Cleveland J P, Callahan R C and Viani M B 2004 *Nanotechnology* **15** 1344–50
[29] Sader J E, Chon J W M and Mulvaney P 1999 *Rev. Sci. Instrum.* **70** 3967
[30] Golovko D S, Haschke T, Wiechert W and Bonaccurso E 2007 *Rev. Sci. Instrum.* **78** 043705
[31] Cleveland J P, Manne S, Bocek D and Hansma P K 1993 *Rev. Sci. Instrum.* **64** 403
[32] Higgins M J, Proksch R, Sader J E, Polcik M, Mc Endoo S, Cleveland J P and Jarvis S P 2006 *Rev. Sci. Instrum.* **77** 013701
[33] Beaulieu L Y, Godin M, Laroche O, Tabard-Cossa V and Grütter P 2006 *Appl. Phys. Lett.* **88** 083108
[34] Schäffer T E, Richter M and Viani M B 2000 *Appl. Phys. Lett.* **76** 3644
[35] Schäffer T E 2002 *J. Appl. Phys.* **91** 4739
[36] Hoffmann A, Jungk T and Soergel E 2007 *Rev. Sci. Instrum.* **78** 016101
[37] Schäffer T E 2005 *Nanotechnology* **16** 664–70
[38] Poggi M A, McFarland A W, Colton J S and Bottomley L A 2005 *Anal. Chem.* **77** 1192–5
[39] Pirzer T and Hugel T 2009 *Rev. Sci. Instrum.* **80** 035110
[40] Thormann E, Pettersson T and Claesson P M 2009 *Rev. Sci. Instrum.* **80** 093701
[41] Beaulieu L Y, Godin M, Laroche O, Tabard-Cossa V and Grütter P 2007 *Ultramicroscopy* **107** 422–30
[42] Lee E J, Park Y, Kim C S and Kouh T 2010 *Curr. Appl. Phys.* **10** 834–7
[43] Burnham N A, Chen X, Hodges C S, Matei G A, Thoreson E J, Roberts C J, Davies M C and Tendler S J B 2003 *Nanotechnology* **14** 1–6
[44] Butt H-J and Jaschke M 1995 *Nanotechnology* **6** 1–7
[45] Gibson C T, Watson G S and Myhra S 1996 *Nanotechnology* **7** 259–62
[46] LeDue J M, Lopez-Ayon M, Miyahara Y, Burke S A and Grütter P 2010 *J. Vac. Sci. Technol.* B **28** C4–C15
[47] Meyer G and Amer N M 1988 *Appl. Phys. Lett.* **53** 1045–7
[48] Martin Y, Williams C C and Wickramasinghe H K 1987 *J. Appl. Phys.* **61** 4723
[49] Alexander S, Hellemans L, Marti O, Schneir J, Elings V, Hansma P K, Longmire M and Gurley J 1989 *J. Appl. Phys.* **65** 164–7
[50] Putman C, Degrooth B, Vanhulst N and Greve J 1992 *Ultramicroscopy* **42–44** 1509–13
[51] Putman C A J, De Grooth B G, Van Hulst N F and Greve J 1992 **72** 6
[52] García-Valenzuela A and Diaz-Uribe R 1997 *Appl. Opt.* **36** 4456–62
[53] García-Valenzuela A 1997 *J. Appl. Phys.* **82** 985
[54] García-Valenzuela A, Sandoval-Romero G E and Sánchez-Pérez C 2004 *Appl. Opt.* **43** 4311–21
[55] Villatoro J and García-Valenzuela A 1999 *Appl. Opt.* **38** 4837–44
[56] García-Valenzuela A 1997 *Opt. Eng.* **36** 1770
[57] García R 2002 *Surf. Sci. Rep.* **47** 197–301
[58] Labuda A, Paul W, Pietrobon B, Lennox R B, Grütter P H and Bennewitz R 2010 *Rev. Sci. Instrum.* **81** 083701
[59] Yurtsever A, Gigler A M, Macias E and Stark R W 2007 *Appl. Phys. Lett.* **91** 253120

[60] Rubio-Sierra F J, Vazquez R and Stark R W 2006 *IEEE Trans. Nanotechnol.* **5** 692–700
[61] Stark M, Guckenberger R, Stemmer A and Stark R W 2005 *J. Appl. Phys.* **98** 114904
[62] Bhushan B 2004 *Springer Handbook of Nanotechnology* (Heidelberg: Springer) p 621
[63] Tur M, Shafir E and Blgtekjaer K 1990 *Lightwave* **8** 183–9
[64] García-Valenzuela A and Villatoro J 1998 *J. Appl. Phys.* **84** 58
[65] Rumyantsev S L, Shur M S, Bilenko Y, Kosterin P V and Salzberg B M 2004 *J. Appl. Phys.* **96** 966
[66] Bhushan B 2011 *Nanotribology and Nanomechanics I* (Berlin: Springer) p 199
[67] Brophy J J 1967 *J. Appl. Phys.* **38** 2465
[68] Callen H B and Welton T A 1951 *Phys. Rev.* **83** 34–40
[69] Callen H and Greene R 1952 *Phys. Rev.* **86** 702–10
[70] Sader J E 1998 *J. Appl. Phys.* **84** 64
[71] Chon J W M, Mulvaney P and Sader J E 2000 *J. Appl. Phys.* **87** 3978
[72] Paul M and Cross M 2004 *Phys. Rev. Lett.* **92** 1–4
[73] Clark M T, Cleveland J P and Paul M R 2010 *Phys. Rev.* E **81** 1–10
[74] Albrecht T R, Grutter P, Horne D and Rugar D 1991 *J. Appl. Phys.* **69** 668–73
[75] Zener C 1937 *Phys. Rev.* **52** 230–5
[76] Sandberg R, Mølhave K, Boisen A and Svendsen W 2005 *J. Micromech. Microeng.* **15** 2249–53
[77] Sosale G, Das K, Fréchette L and Vengallatore S 2011 *J. Micromech. Microeng.* **21** 105010
[78] Prabhakar S and Vengallatore S 2007 *J. Micromech. Microeng.* **17** 532–8
[79] Kobayashi K, Yamada H and Matsushige K 2009 *Rev. Sci. Instrum.* **80** 043708
[80] Dürig U, Steinauer H R and Blanc N 1997 *J. Appl. Phys.* **82** 3641
[81] Giessibl F J 2003 *Rev. Mod. Phys.* **75** 949–83
[82] Polesel-Maris J and Gauthier S 2007 *J. Phys.: Conf. Ser.* **61** 949–54
[83] Lübbe J, Troger L, Torbrugge S, Bechstein R, Richter C, Kuhnle A and Reichling M 2010 *Meas. Sci. Technol.* **21** 125501
[84] Colchero J, Cuenca M, González Martínez J F, Abad J, Pérez García B, Palacios-Lidón E and Abellán J 2011 *J. Appl. Phys.* **109** 024310
[85] Kimball A and Lovell D 1927 *Phys. Rev.* **30** 948–59
[86] Walther H 1935 *Sci. Mon.* **41** 275
[87] Paolino P and Bellon L 2009 *Nanotechnology* **20** 405705
[88] Kiracofe D, Kobayashi K, Labuda A, Raman A and Yamada H 2011 *Rev. Sci. Instrum.* **82** 013702
[89] Ramos D, Tamayo J, Mertens J and Calleja M 2006 *J. Appl. Phys.* **99** 124904
[90] von Fraunhofer J 1825 *Theorie Der Höfe, Nebensonnen Und Verwandter Phänomene Mit Versuchen Zur Bestätigung Derselben*
[91] Fresnel A-J 1819 *Mémoire Sur La Diffraction De La Lumière* (Paris: Mémoires de l'Académie des sciences de l'Institut de France)
[92] Teich M C and Saleh B E A 1991 *Fundamentals of Photonics* (New York: Wiley) p 85
[93] Schäffer T E and Fuchs H 2005 *J. Appl. Phys.* **97** 083524
[94] Hecht E 2002 *Optics* (Reading, MA: Addison-Wesley) p 154
[95] Xia L, Wu W, Xu J, Hao Y and Wang Y 2006 *MEMS 2006: 19th IEEE Int. Conf. on Micro Electro Mechanical Systems, 2006 (Istanbul, IEEE)* pp 118–21
[96] Nebiker P W, Döbeli M, Mühle R and Suter M 1997 *Nucl. Instrum. Methods Phys. Res.* B **127-128** 897–900
[97] Hecht E 2002 *Optics* (Reading, MA: Addison-Wesley) p 495
[98] Green M A and Keevers M J 1995 *Prog. Photovolt., Res. Appl.* **3** 189–92
[99] Johnson P B and Christy R W 1972 *Phys. Rev.* B **6** 4370–9
[100] Palik E D 1991 *Handbook of Optical Constants of Solids* (New York: Academic)